# A Tunable Split Resonator Method for Nondestructive Permittivity Characterization

Xiangyi Fang, David Linton, Chris Walker, and Brian Collins

*Abstract*—The split cylinder resonator method is improved for nondestructive and accurate measurement for low permittivity materials at multiple frequency points. The dielectric constants of flat substrate materials are calculated based on a rigorous mode match analysis of the $TE_{011}$ mode. The loss tangent is also approximately calculated. The dielectric properties of two commercial substrates have been measured at multiple frequencies. The results demonstrate that this technology is capable of accurately characterizing the dielectric properties of flat substrate materials versus frequency in a nondestructive way.

*Index Terms*—Cavity resonator, dielectric materials, microwave measurement, nondestructive testing, permittivity measurement.

## I. INTRODUCTION

THE SUBSTRATE materials used in microstrip antennas and RF/microwave circuits demand low dielectric constant and low dielectric loss. The design and fabrication of patch antennas and microstrip circuits often require accurate characterization of the substrate parameters. For online quality control in substrate manufacturing and processing, it is also necessary to develop a nondestructive method for dielectric measurement.

The open-end coaxial probe method [1], [2] is a nondestructive and broadband technique for dielectric property measurement. However, it is not accurate enough, especially for low dielectric constant and low-loss materials. The transmission line method [3] has better accuracy than the open-end coaxial method for dielectric measurement. However, test samples have to be accurately machined. Any size error of the sample would result in a considerable uncertainty in dielectric measurement. Resonator methods are well known as the most accurate method for dielectric measurement at microwave frequencies. However, they generally require the sample to be machined accurately into a suitable geometry to fit the resonant cavity. That is often difficult for some materials, such as ceramics, and certainly undesirable for nondestructive testing.

Kent [4] developed a split resonator technique that allows for nondestructive measurements of complex permittivity. The split-cylinder resonator is composed of two cylindrical waveguides with their terminals shorted. The substrate sheet is inserted in the gap between the two shorted cylindrical cavities. The complex permittivity of the substrate is determined from measurement of the resonant frequency and the quality factor of the $TE_{011}$ resonant mode. In terms of sample geometry, the only requirement is that the samples must extend beyond the diameter of the cylindrical cavity sections and the sample must be planar. This provides the accuracy of a resonator technique without having to machine the test specimens. However, the calculation process of permittivity is complex for this situation because of the open cavity structure. In the closed resonator method, the electromagnetic field is restricted within a metallic cavity and the boundary problem is relatively simple. While, for the split-cylinder resonator, because of a gap existing between two cylindrical waveguide sections, it is troublesome for electromagnetic field resolution and permittivity calculation. Kent and Baker [5] proposed an approximate correction to the measured permittivity based on a perturbation calculation. The calculation, however, requires a complex iterative process. Janezic *et al.* [6] presented a full-wave analysis of the split cylinder resonator. The model includes the $TE_{011}$ resonant mode plus evanescent $TE_{0n}$ modes in the cylindrical cavity region. This approach gives a rigorous and well-defined expression for dielectric constant calculation. Including $TE_{0n}(n > 1)$ modes causes the permittivity extraction process to be very complicated.

In general, the dielectric properties of materials vary versus frequency and measurement of them must be performed at the application frequency. For the fixed-frequency split cylinder resonator, both different dielectric constant and different thickness of sample can result in a different resonant frequency each time, which is generally not at the application frequency of interest. To perform measurement at its application frequency, the resonant frequency of the split resonator should be tunable.

This investigation improves the split resonator method so as to make it capable of accurately measuring dielectric properties of low dielectric constant materials at multiple frequencies instead of at only one frequency. A simpler way of deriving the equation is also proposed in this investigation for calculating $\varepsilon_r$ in a split resonator based on the rigorous mode match method. The principle drawing is shown in Fig. 1(a) and the experimental construction is shown in Fig. 1(b). Two moveable plates are set in the two cylindrical cavities as the terminations, which can be moved by vernier positioners, respectively. Thus, the resonant frequency of the split resonator can be tunable by symmetrically moving the end plate positions. The $TE_{011}$ resonant frequency is obtained by measuring the S parameters versus frequency from the Agilent 8510B network analyzer. The dielectric constant is then extracted by considering only the $TE_{011}$ resonant mode in the mode match analysis. The dimensions of the fabricated test apparatus are $a = 35.01 \pm 0.01$ mm and $L = 52.01 \pm 0.01$ mm.
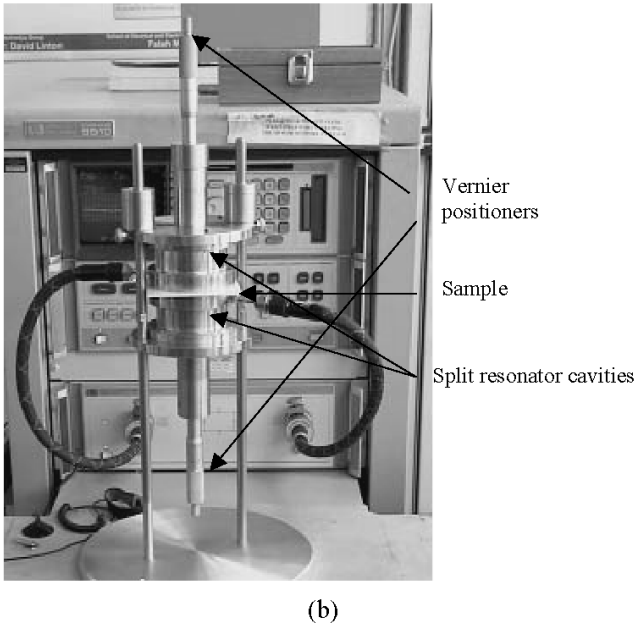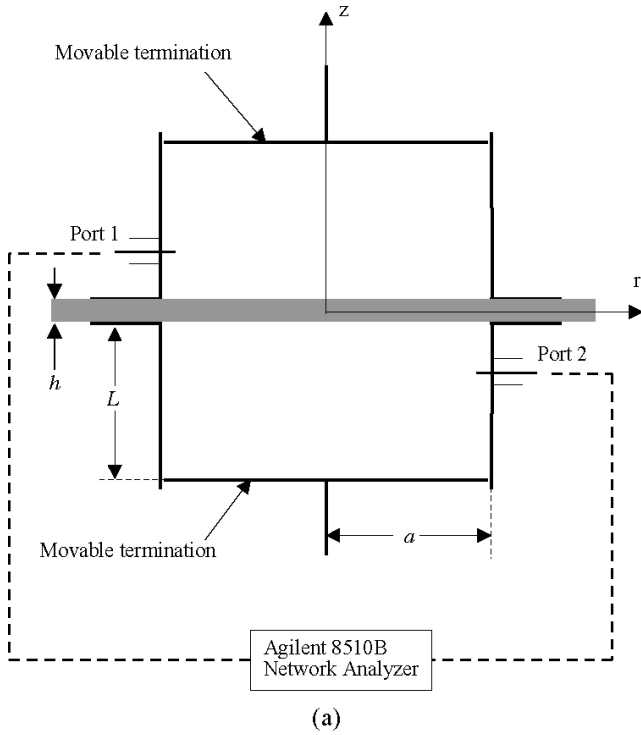
Fig. 1. Tunable split cylinder resonator. (a) Principle drawing. (b) Experimental construction.

Two commercial substrates have been measured at multiple frequencies.

## II. PERMITTIVITY MEASUREMENT STRATEGY

In Fig. 1(a), the $z$ component of standing magnetic field of the $TE_{011}$ mode in the upper cavity region can be expressed as follows [4], [6]:

$$H_z = H_0 J_0 \left( \frac{x_{01}}{a} r \right) \sin \left[ \beta_0 \left( L + \frac{h}{2} - z \right) \right]. \quad (1)$$

The other components can be derived from $H_z$ [7]

$$
\begin{aligned}
H_r &= \left( \frac{a}{x_{01}} \right)^2 \frac{\partial^2 H_z}{\partial z \partial r} \\
&= -H_0 \frac{a}{x_{01}} \beta_0 J_1 \left( \frac{x_{01}}{a} r \right) \cos \left[ \beta_0 \left( L + \frac{h}{2} - z \right) \right] \quad (2)
\end{aligned}
$$

$$
\begin{aligned}
E_\varphi &= \frac{j \omega \mu_0 a^2}{x_{01}^2} \frac{\partial H_z}{\partial r} \\
&= j \omega \mu_0 H_0 \frac{a}{x_{01}} J_1 \left( \frac{x_{01}}{a} r \right) \sin \left[ \beta_0 \left( L + \frac{h}{2} - z \right) \right] \quad (3)
\end{aligned}
$$

$$\beta_0{}^2 = \omega^2 \mu_0 \varepsilon_0 - \left( \frac{x_{01}}{a} \right)^2. \quad (4)$$

In the above equations, $J_0$ and $J_1$ are, respectively, the Bessel functions of the first kind of order zero and order one; $H_0$ is a constant representing the maximum magnitude of the magnetic field strength in the $z$ direction of the cavity; $x_{01}$ is the first root of $J_0'(r) = 0$, which has a value of 3.831 71; $a$ is the inner radius of the split cavities and $h$ is the thickness of the substrate sample. The $\mu_0$ and $\varepsilon_0$ are the vacuum permeability and permittivity respectively. $\omega$ is the angular resonant frequency of the $TE_{011}$ mode.

The transverse field in the sample region can be expressed as follows for the $TE_{011}$ mode:

$$H_z^s = H_s J_0(\lambda r) \cos(\beta z) \quad (5)$$

$$H_r^s = H_s \frac{\beta}{\lambda} J_1(\lambda r) \sin(\beta z) \quad (6)$$

$$E_\varphi^s = -H_s \frac{j \omega \mu_0}{\lambda} J_1(\lambda r) \cos(\beta z) \quad (7)$$

$$\beta^2 = \omega^2 \mu_0 \varepsilon_0 \varepsilon_r - \lambda^2. \quad (8)$$

The $\lambda$ is the continuous radial eigenvalue, $H_s$ is the constant presenting the maximum magnitude of the magnetic field strength in the $z$ direction in the sample, and $\varepsilon_r$ is the dielectric constant of the sample.

Matching the interface condition on the interface between air and the sample

$$E_\varphi \left( \frac{h}{2} \right) = E_\varphi^s \left( \frac{h}{2} \right) \quad (9)$$

$$H_r \left( \frac{h}{2} \right) = H_r^s \left( \frac{h}{2} \right). \quad (10)$$

The following equations are then obtained:

$$
\begin{aligned}
H_0 \frac{j \omega \mu_0 a}{x_{01}} J_1 &\left( \frac{x_{01}}{a} r \right) \sin(\beta_0 L) \\
&= H_s \frac{j \omega \mu_0}{\lambda} J_1(\lambda r) \cos \left( \beta \frac{h}{2} \right) \quad (11)
\end{aligned}
$$

$$
\begin{aligned}
H_0 \frac{a \beta_0}{x_{01}} J_1 &\left( \frac{x_{01}}{a} r \right) \cos(\beta_0 L) \\
&= H_s \frac{\beta}{\lambda} J_1(\lambda r) \sin \left( \beta \frac{h}{2} \right) \quad (12)
\end{aligned}
$$

Combining (11) and (12), we can obtain the following equation:

$$\beta_0 \cot(\beta_0 L) = \beta \tan \left( \beta \frac{h}{2} \right). \quad (13)$$

In order to eliminate the radial eigenvalue $\lambda$ and obtain an equation just containing relative dielectric constant, we take the Hankel transform and then the inverse Hankel transform of (13). The Hankel transform used here is defined as

$$\overline{f}(\lambda) = \int_0^\infty r f(r) J_1(\lambda r) dr. \tag{14}$$

The inverse Hankel transform is

$$f(r) = \int_0^\infty \lambda \overline{f}(\lambda) J_1(\lambda r) d\lambda. \tag{15}$$

Performing the Hankel and inverse Hankel transform of (13), (16) can be obtained

$$\beta_0 \cot(\beta_0 L) = \int_0^\infty \int_0^a \beta \tan\left(\beta \frac{h}{2}\right) J_1(\lambda r) r dr J_1(r\lambda) \lambda \, d\lambda. \tag{16}$$

Multiplying both sides of (16) by $J_1(r)^2 \cdot r$ and integrating over the interval [0,a]

$$\beta_0 \cot(\beta_0 L) \frac{a^2}{2} J_0^2(x_{01}) = \int_0^\infty \beta \tan\left(\beta \frac{h}{2}\right)$$
$$\times \left[\int_0^a J_1(\lambda r) J_1\left(\frac{x_{01}}{a} r\right) r dr\right]^2 \lambda d\lambda. \tag{17}$$

Performing the integration in the square bracket of (17) by making use of the relation [8]

$$\int_0^x J_n(k \cdot x) \cdot J_n(l \cdot x) \cdot x \cdot dx = \frac{x}{k^2 - l^2}$$
$$\cdot [k \cdot J_n(l \cdot x) J_{n+1}(k \cdot x) - l \cdot J_n(k \cdot x) J_{n+1}(l \cdot x)].$$

That is

$$\int_0^a J_1(\lambda r) J_1\left(\frac{x_{01}}{a} r\right) r dr = \frac{-a}{\lambda^2 - \left(\frac{x_{01}}{a}\right)^2} \frac{x_{01}}{a} J_1(\lambda a) J_2(x_{01})$$

using the relation $J_2(x_{01}) = -J_0(x_{01})$.

Equation (17) becomes

$$\frac{1}{2}\beta_0 \cot \beta_0 L - \left(\frac{x_{01}}{a}\right)^2 \int_0^\infty \beta \tan\left(\beta \frac{h}{2}\right) \left[\frac{J_1(\lambda a)}{\lambda^2 - \left(\frac{x_{01}}{a}\right)^2}\right]^2 \lambda d\lambda = 0. \tag{18}$$

$\varepsilon_r$ is the only variable in (18). Thus, the permittivity $\varepsilon_r$ can be obtained from (18) by an iterative calculation process when the resonant frequency of $TE_{011}$ is measured.

In order to verify the accuracy of the improved split cylinder resonator, shaped circular samples with the same radius as the cylindrical cavity were fitted into a closed cavity and their permittivity was measured. For the closed cylindrical cavity, the $\varepsilon_r$ can be calculated from (19) [4]

$$\theta \tan\left(\theta \cdot \frac{d}{2}\right) - \theta_0 \cot(\theta_0 L) = 0. \tag{19a}$$

In (19)

$$\theta_0^2 = \omega^2 \mu_0 \varepsilon_0 - \left(\frac{x_{01}}{a}\right)^2 \tag{19b}$$

$$\theta^2 = \omega^2 \mu_0 \varepsilon_0 \varepsilon_r - \left(\frac{x_{01}}{a}\right)^2. \tag{19c}$$

The quality factor of the system is defined as follows [6]:

$$Q = \frac{\omega(w_c + w_s)}{P_c + P_l + P_s}. \tag{20}$$

In the above equation, $w_c$ and $w_s$ are the average energy stored in the cavity section and sample. $P_c$, $P_l$, and $P_s$ are the power dissipation per second in the cavity walls, coupling loops and sample. Rearranging (20), the following expression can be obtained:

$$\frac{1}{Q} = \frac{P_c + P_l}{\omega(w_c + w_s)} + \frac{P_s}{\omega(w_c + w_s)} = \frac{1}{Q_{cl}} + \frac{1}{Q_s}. \tag{21}$$

$Q_{cl}$ is the quality factor due to the losses in the cavity wall and loops and $Q_s$ is the quality factor due to loss in the sample. To evaluate $Q_{cl}$ requires complicated time consuming integrations. We approximately take the measured quality factor of the empty closed cavity as $Q_{cl}$. From experiment, it was found that $Q_{cl}$ is one order of magnitude larger than $Q$. Then, $1/Q_{cl}$ could reasonably be assumed to be negligible in (21). Hence, the measured quality factor $Q$ is mainly due to $Q_s$. Thus, the loss tangent could be obtained from the measured $Q$ [6]

$$\tan \delta = \frac{1}{Q} = \frac{\Delta f}{f_r} \tag{22}$$

where $\Delta f$ and $f_r$ are the $-3$-dB bandwidth of the insertion loss and resonant frequency, respectively.

The uncertainty $\Delta \varepsilon_r$ results from the uncertainties of the resonant frequency, sample thickness, diameter, and length of the resonator cavity. It can be expressed by (23), as seen at the bottom of the page. All items in (23) could be numerically calculated using (18) by giving perturbations $\Delta f_r$, $\Delta h$, $\Delta L$, and $\Delta a$, respectively. Thus, $\Delta \varepsilon_r$ can be obtained using (23).

## III. EXPERIMENTAL RESULTS

The complex permittivity of two kinds of low-loss substrate samples have been measured using the tunable split cylinder resonator method. Taconic-TLC-32 and Rogers-RO3010 commer-

$$\Delta \varepsilon_r = \sqrt{\left(\frac{\partial \varepsilon_r}{\partial f_r} \cdot \Delta f_r\right)^2 + \left(\frac{\partial \varepsilon_r}{\partial h} \cdot \Delta h\right)^2 + \left(\frac{\partial \varepsilon_r}{\partial L} \cdot \Delta L\right)^2 + \left(\frac{\partial \varepsilon_r}{\partial a} \cdot \Delta a\right)^2} \tag{23}$$
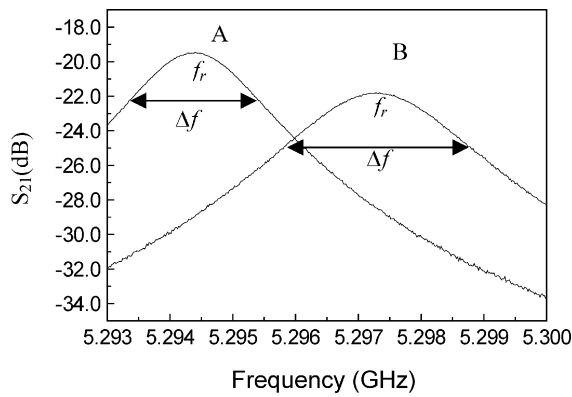
Fig. 2.   Resonance curves measured by (A) the split resonator and (B) the closed resonator for Taconic-TLC-32 substrate.
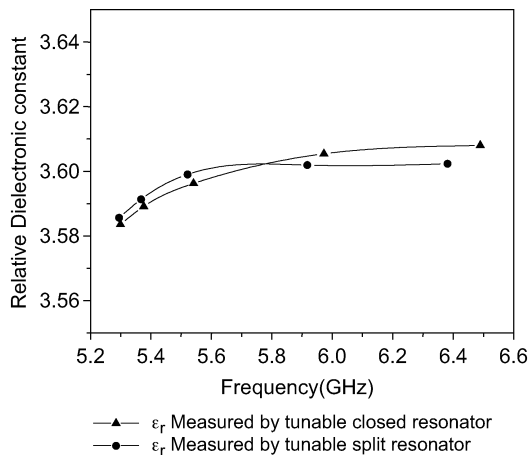


Fig. 3.   $\varepsilon_r$ versus frequency of commercial TLC-32 substrate measured by tunable split and closed resonators, respectively.
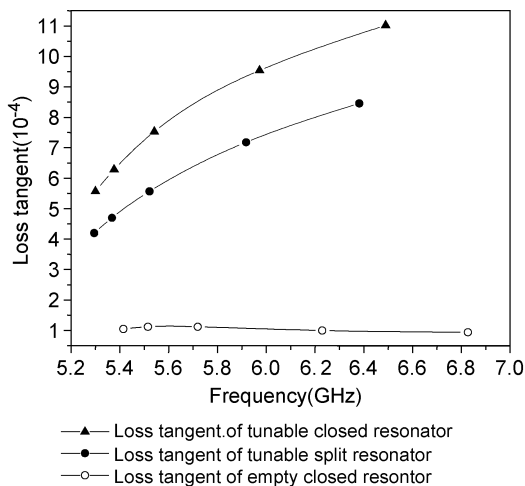


Fig. 4.   $\tan \delta$ versus frequency of TLC-32 sample loaded tunable split and closed resonators, and that of the empty closed resonator.

cial copper-clad substrates were used and the copper foils on both sides of the substrate materials were all removed by chemical etching. The samples, with a diameter larger than that of the cylindrical cavity, were inserted into the gap of the split cylinder resonator. According to [6], the larger the $\varepsilon_r$ and thickness of the
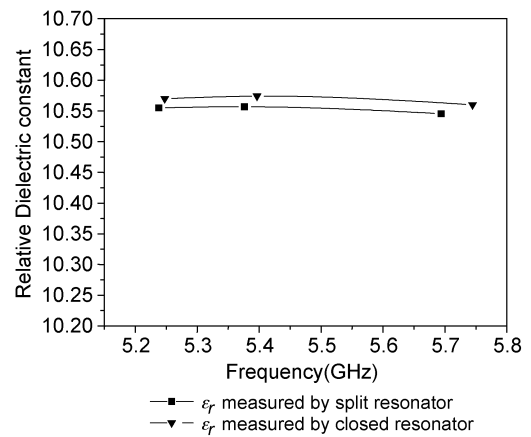


Fig. 5.   $\varepsilon_r$ versus frequency of commercial RO3010 substrate measured by split and closed resonators, respectively.
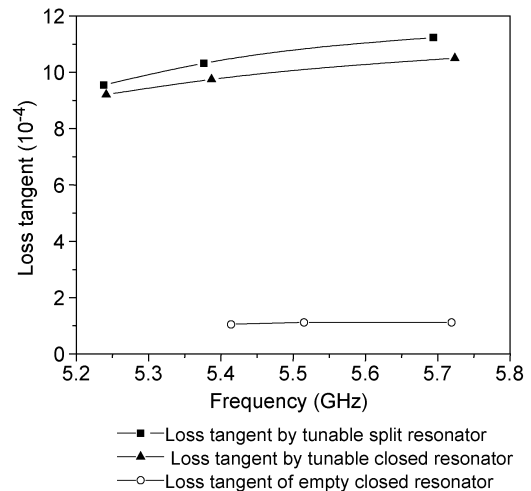


Fig. 6.   $\tan \delta$ versus frequency of RO3010 sample loaded tunable split and closed resonators, and that of the empty closed resonator.
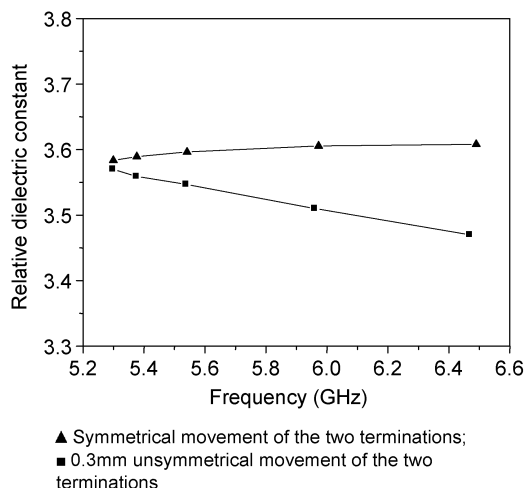


Fig. 7.   $\varepsilon_r$ versus frequency of TLC-32 substrate measured by tunable split resonators with symmetrical and unsymmetrical movement of the two terminations.

sample sheet are, the further the electric field $\left(E_\varphi^S\right)$ will spread from the edge of the cylindrical cavity into the flange coupling

TABLE I
RELATIVE DIELECTRIC CONSTANTS AND LOSS TANGENTS OF TLC-32 SUBSTRATE MEASURED USING TUNABLE SPLIT AND CLOSED CYLINDER
RESONATORS, AND THE LOSS TANGENT OF THE EMPTY CYLINDRICAL CAVITY. THE THICKNESS OF THE SAMPLE IS $0.778 \pm 0.002$ mm

| Split-cylinder resonator | | | Closed cylindrical cavity | | | Empty closed cylinder cavity | |
|---|---|---|---|---|---|---|---|
| $f_r$ (GHz) | $\varepsilon_r$ | $\tan\delta$ $(10^{-4})$ | $f_r$ (GHz) | $\varepsilon_r$ | $\tan\delta$ $(10^{-4})$ | $f_r$ (GHz) | $\tan\delta$ $(10^{-4})$ |
| 5.29471 $\pm 0.00004$ | 3.586 $\pm 0.027$ | 4.2 $\pm 0.2$ | 5.29935 $\pm 0.00004$ | 3.584 $\pm 0.027$ | 5.6 $\pm 0.7$ | 5.41406 | 1.05 |
| 5.36765 $\pm 0.00006$ | 3.591 $\pm 0.029$ | 4.7 $\pm 0.2$ | 5.37648 $\pm 0.00003$ | 3.589 $\pm 0.029$ | 6.3 $\pm 0.9$ | 5.51497 | 1.12 |
| 5.52151 $\pm 0.00004$ | 3.599 $\pm 0.026$ | 5.6 $\pm 0.2$ | 5.54115 $\pm 0.00005$ | 3.596 $\pm 0.034$ | 7.5 $\pm 0.8$ | 5.71898 | 1.12 |
| 5.91733 $\pm 0.00005$ | 3.602 $\pm 0.027$ | 7.2 $\pm 0.2$ | 5.97275 $\pm 0.00003$ | 3.605 $\pm 0.028$ | 9.5 $\pm 0.8$ | 6.22926 | 1 |
| 6.38143 $\pm 0.00005$ | 3.602 $\pm 0.026$ | 8.5 $\pm 0.2$ | 6.48968 $\pm 0.00005$ | 3.608 $\pm 0.035$ | 11.0 $\pm 0.7$ | 6.82671 | 0.94 |

region. The noted $\varepsilon_r$ and $\tan\delta$ of Taconic-TLC-32 substrate at 10 GHz are $3.20 \pm 0.05$ and 0.003 respectively. Its thickness is measured to be $0.778 \pm 0.002$ mm. The noted $\varepsilon_r$ and $\tan\delta$ of Rogers-RO3010 substrate at 10 GHz are $10.2 \pm 0.3$ and 0.0035, respectively. Its thickness is measured to be $0.655 \pm 0.002$ mm. For such thicknesses, the electric field would almost vanish when $r$ extends to $1.05a$ [6] in the sample. In our measurement, the width of the samples has been taken to be more than 100 mm, that is more than $2.6a$ (a $= 35$ mm). Thus, it is large enough to ensure the electric field vanishes in the sample. The resonant frequencies and $-3$-dB bandwidth of the resonant curve of $TE_{011}$ modes were obtained by measuring $S_{21}$ versus frequency using an Agilent 8510B network analyzer.

Tuning the movable terminal plates symmetrically, the resonant frequency is changed and the permittivity at several frequencies can be obtained. Fig. 1(b) shows the measurement construction. The $TM_{11p}$ (p $= 1, 2, 3, \ldots$) modes are suppressed by the gap between the cylinder cavity walls and the movable terminations. The $S_{21}$ resonant magnitude of the $TE_{01p}$ mode has not been influenced because there is no surface current flowing across the gap for the field characteristics of the $TE_{01p}$ mode [7]. The $TE_{011}$ mode is the only one of interest in our measurement and its resonant frequency changes with the movement of the two terminations.

Fig. 2 shows an example of the $S_{21}$ curves from which the $TE_{011}$ resonant frequency and quality factor $Q$ could be extracted, and, thus, $\varepsilon_r$ can be determined using (18), (19), respectively, for split and closed cylinder resonators and $\tan\delta$ can be determined using (22). It can be seen that the resonant frequency of the split resonator is slightly lower than that of the closed resonator. The difference of the resonant frequencies between split and closed resonators depends on the differences of thickness and dielectric constant of the measured substrate.

Fig. 3 illustrates the dielectric constants versus frequency of the TLC-32 substrate for both cases of the split and closed cylinder resonator methods. It is shown that the results of the two methods are very consistent with each other. Thus, using the tunable split resonator method, the relationship of dielectric constant versus frequency is accurately measured for low dielectric constant materials without the requirement

TABLE II
RELATIVE DIELECTRIC CONSTANTS AND LOSS TANGENTS OF RO3010 SUBSTRATE MEASURED USING TUNABLE SPLIT AND CLOSED CYLINDER RESONATORS. THE THICKNESS OF THE SAMPLE IS $0.655 \pm 0.002$ mm

| Split-cylinder resonator | | | Closed cylindrical cavity | | |
|---|---|---|---|---|---|
| $f_r$ (GHz) | $\varepsilon_r$ | $\tan\delta$ $(10^{-4})$ | $f_r$ (GHz) | $\varepsilon_r$ | $\tan\delta$ $(10^{-4})$ |
| 5.23775 $\pm 0.00006$ | 10.55 $\pm 0.03$ | 9.55 $\pm 0.5$ | 5.24748 $\pm 0.00005$ | 10.57 $\pm 0.03$ | 9.2 $\pm 2.1$ |
| 5.37615 $\pm 0.00005$ | 10.56 $\pm 0.03$ | 10.32 $\pm 0.4$ | 5.39665 $\pm 0.00004$ | 10.58 $\pm 0.03$ | 9.8 $\pm 1.9$ |
| 5.69378 $\pm 0.00005$ | 10.55 $\pm 0.03$ | 11.23 $\pm 0.4$ | 5.74445 $\pm 0.00005$ | 10.56 $\pm 0.03$ | 10.5 $\pm 1.9$ |

of destructive sample preparation but with the accuracy of the closed cavity method.

Fig. 4 shows the loss tangents of the sample loaded tunable split and closed cylinder resonators, and of the empty closed resonator versus frequency. The loss tangent $\tan\delta$ of the loaded closed cylinder resonator is somewhat larger than that of the loaded split cylinder resonator. Both results indicate increasing relative permittivity with the increase of frequency. The $\tan\delta$ of the empty resonator is no more than $1.2 \times 10^{-4}$ and reduces with increasing frequency.

Fig. 5 shows the dielectric constant versus frequency of commercial RO3010 for the cases of both the split and closed cylinder resonator methods. From Figs. 3 and 5, it can be seen that there is a similar dielectric constant divergence measured using the tunable split and closed cylinder resonators for both high permittivity (such as RO3010) and low permittivity materials (such as TLC-32).

Fig. 6 shows the loss tangent of RO3010 substrate measured by tunable split and closed cylindrical resonators versus frequency, respectively. The $\tan\delta$ of the empty closed resonator is also shown in Fig. 6 for comparison. It can be seen when comparing Figs. 4 and 6 that, for high permittivity materials (such as RO3010), the loss tangent divergence measured by the split and closed resonator methods is smaller than that of low permittivity materials (such as TLC-32).

It is found that the unsymmetrical movement of the two terminations can result in a considerable measurement error. Fig. 7 shows the $\varepsilon_r$ measurement divergence when there is 0.3-mm difference between the movements of the two terminations. The error will become larger with increasing frequency. This is caused by the unsymmetrical movements of the two terminations making the sample depart from the central position of the electric field of the $TE_{011}$ mode. Thus, symmetrical movement of the two terminations is required in this measurement procedure.

All measured results and uncertainties are summarized in Tables I and II, respectively, for Taconic-TLC-32 and Rogers-RO3010 substrates.

## IV. CONCLUSION

For the purpose of nondestructive and accurate permittivity measurement of dielectric substrates versus frequency, the split cylinder resonator has been significantly improved so that the resonant frequency becomes tunable. A theoretical model has also been set up for calculating the permittivity with a rigorous mode match method. The open character of the field is considered, and only the $TE_{011}$ mode is taken into account in experimental measurement and calculation.

Using the tunable split cylinder resonator and the simplified calculation equation, the permittivity of some dielectric substrates has been determined versus frequency. For comparison, the same substrate materials were also measured with a closed resonator. The results of the two methods agree well with each other.

## ACKNOWLEDGMENT

## REFERENCES

[1] D. K. Misra, "A quasistatic analysis of open-end coaxial lines," *IEEE Trans. Microwave Theory Tech.*, vol. MTT-35, pp. 925–928, Oct. 1987.
[2] ——, "On the measurement of the complex permittivity of materials by an open-end coaxial probe," *IEEE Microwave Guided Wave Lett.*, vol. 5, pp. 161–163, May 1995.
[3] I. J. Youngs, "NAMAS-accredited microwave permittivity/permeability measurement system," *Proc. Inst. Elect. Eng.*, vol. 143, no. 4, pp. 247–253, July 1996.
[4] G. Kent, "Nondestructive permittivity measurement of substrates," *IEEE Trans. Instrum. Meas.*, vol. 45, pp. 102–106, Feb. 1996.
[5] G. Kent and S. M. Bell, "The gap correction for the resonant mode dielectrometer," *IEEE Trans. Instrum. Meas.*, vol. 45, pp. 98–101, Feb. 1996.
[6] M. D. Janezic and J. Baker-Jarvis, "Full wave analysis of a split-cylinder resonator for nondestructive permittivity measurements," *IEEE Trans. Microwave Theory Tech.*, vol. 47, pp. 2014–2020, Oct. 1999.
[7] D. Kajfez and P. Guillon, *Dielectric Resonator*. Norwood, MA: Artech House, 1986, p. 40.
[8] R. E. Collin, *Foundations for Microwave Engineering*. New York: McGraw-Hill, 1966.

**Xiangyi Fang** received the B.S. degree in physics and the M.S. and Ph.D. degrees in electronic materials from the Xian Jiaotong University, China, in 1982, 1987, and 2000, respectively.

He is currently a Research Fellow with the School of Electrical and Electronic Engineering, Queen's University, Belfast, U.K. His research interests include the characterization of dielectric materials in RF/microwave frequency, the fabrication and characterization of high-density interconnection circuits, ferroelectrics, and gas and chemical sensors.

**David Linton** received the B.Sc. degree (first class honors) in electrical engineering and the Ph.D. degree in high-frequency interconnect modeling from Queen's University, Belfast, U.K., in 1983 and 1992, respectively.

He was with Lucas Industries as a Project Engineer, Project Leader, and Applications Manager. He has over ten years of experience working in the design and manufacture of thick-film microcircuits and surface mount PCBs for the telecommunications and automotive industries. He has worked in design, manufacture, quality assurance, R&D, and customer applications engineering. In 1989, he returned to Queen's University as a Lecturer. He is currently a Senior Lecturer with the School of Electrical and Electronic Engineering, Queen's University, and is Deputy Director of the High Frequency Electronics Group (HFEG). He has published 70 journal and conference papers. His interests include microwave/RF measurements, RF component development for low-cost packaging, electromagnetic modeling, and high-speed pulse sources and samplers using NLTL techniques.

**Chris Walker**, photograph and biography not available at the time of publication.

**Brian Collins**, photograph and biography not available at the time of publication.